Brain-wide genetic mapping identifies the indusium griseum as a prenatal target of pharmacologically unrelated psychostimulants

Janos Fuzik[a,b], Sabah Rehman[a,1], Fatima Girach[a,1], Andras G. Miklosi[a,1], Solomiia Korchynska[a], Gloria Arque[a], Roman A. Romanov[a], János Hanics[c,d], Ludwig Wagner[e], Konstantinos Meletis[b], Yuchio Yanagawa[f], Gabor G. Kovacs[g], Alán Alpár[c,d], Tomas G. M. Hökfelt[b,2], and Tibor Harkany[a,b,2]

[a]Department of Molecular Neurosciences, Center for Brain Research, Medical University of Vienna, A-1090 Vienna, Austria; [b]Department of Neuroscience, Biomedicum, Karolinska Institutet, SE-17165 Stockholm, Sweden; [c]SE NAP Research Group of Experimental Neuroanatomy and Developmental Biology, Semmelweis University, H-1085 Budapest, Hungary; [d]Department of Anatomy, Histology, and Embryology, Semmelweis University, H-1085 Budapest, Hungary; [e]University Clinic for Internal Medicine III, General Hospital Vienna, A-1090 Vienna, Austria; [f]Department of Genetic and Behavioral Neuroscience, Gunma University Graduate School of Medicine, Maebashi, Gunma 371-8511 Japan; and [g]Neurodegeneration Research Group, Institute of Neurology, Medical University of Vienna, A-1090 Vienna, Austria

Contributed by Tomas G. M. Hökfelt, October 10, 2019 (sent for review March 11, 2019; reviewed by Antonello Bonci, Beat Schwaller, and Carsten T. Wotjak)

Psychostimulant use is an ever-increasing socioeconomic burden, including a dramatic rise during pregnancy. Nevertheless, brain-wide effects of psychostimulant exposure are incompletely understood. Here, we performed Fos-CreER^{T2}–based activity mapping, correlated for pregnant mouse dams and their fetuses with amphetamine, nicotine, and caffeine applied acutely during midgestation. While light-sheet microscopy-assisted intact tissue imaging revealed drug- and age-specific neuronal activation, the indusium griseum (IG) appeared indiscriminately affected. By using GAD67$^{gfp/+}$ mice we subdivided the IG into a dorsolateral domain populated by γ-aminobutyric acidergic interneurons and a ventromedial segment containing glutamatergic neurons, many showing drug-induced activation and sequentially expressing Pou3f3/Brn1 and secretagogin (Scgn) during differentiation. We then combined Patch-seq and circuit mapping to show that the ventromedial IG is a quasi-continuum of glutamatergic neurons (IG-*Vglut1*$^+$) reminiscent of dentate granule cells in both rodents and humans, whose dendrites emanate perpendicularly toward while their axons course parallel with the superior longitudinal fissure. IG-*Vglut1*$^+$ neurons receive VGLUT1$^+$ and VGLUT2$^+$ excitatory afferents that topologically segregate along their somatodendritic axis. In turn, their efferents terminate in the olfactory bulb, thus being integral to a multisynaptic circuit that could feed information antiparallel to the olfactory–cortical pathway. In IG-*Vglut1*$^+$ neurons, prenatal psychostimulant exposure delayed the onset of Scgn expression. Genetic ablation of *Scgn* was then found to sensitize adult mice toward methamphetamine-induced epilepsy. Overall, our study identifies brain-wide targets of the most common psychostimulants, among which *Scgn*$^+$/*Vglut1*$^+$ neurons of the IG link limbic and olfactory circuits.

amphetamine | caffeine | human | nicotine | Patch-seq

Drug abuse is a major socioeconomic burden which affects many age groups and both genders (1, 2). Psychostimulants are among the most widely used drugs, and besides illicit substances like amphetamine and its derivatives include caffeine (coffee) and nicotine (tobacco). Molecular and structural determinants mediating the action of these drugs on neurons differ fundamentally. Amphetamine is excitatory by increasing extracellular dopamine levels through inhibition (or even reversal) of dopamine transport for cellular reuptake (1, 3, 4). Caffeine antagonism at the adenosine A_2A receptor (5) (and less so at A_1 and A_3) is a catalyst for catecholamine (particularly dopamine) and acetylcholine release (6). Nicotine activates ionotropic nicotinic acetylcholine receptors to stimulate synaptic neurotransmission, particularly in the dopaminergic reward circuitry (7). Despite differences in their mechanism of action, a common denominator of psychostimulant action is their ability to prime the brain's reward circuitry to trigger addiction (2). Therefore, any brain region that receives significant dopamine input is at risk upon excess exposure to psychoactive substances.

The consumption of illicit or legal drugs during pregnancy is a primary health concern. Besides counteracting medical conditions, such as hyperemesis gravidarum by cannabis and cannabinoids (8), the use of psychostimulants is reasoned by improving forgetfulness, mood, and stress. Nevertheless, the efficient cross-placental transfer of these structurally distinct compounds (9–11) prompts caution for their direct, indiscriminate, and likely adverse effect, particularly if used repeatedly. Mechanistically, dopaminergic neurons and their long-range projections to the forebrain form during the first trimester of human brain development (12), thereby being poised to modulate the migration and neuritogenesis of telencephalic neurons over long periods (13, 14). Nevertheless, the brain-wide distribution of fetal neurons

Significance

Drug abuse during pregnancy carries significant risk for impaired fetal development. Here, we show that episodic exposure to amphetamine, nicotine, or caffeine during pregnancy induces various patterns of neuronal activity in the fetal brain. The indusium griseum, situated parallel to the central surface of the cortical hemispheres, is indiscriminately activated. Herein, psychostimulants preferentially target glutamatergic neurons and delay their differentiation. Particularly, expression of secretagogin, a Ca^{2+}-sensor protein, is deregulated, which is significant because its loss impairs the integration of information that flows along limbic and olfactory circuits. Cumulatively, we describe psychostimulant-sensitive brain regions and unique neuronal subtypes whose developmental delay disrupts circuit wiring such that behavioral abnormalities can manifest in offspring prenatally exposed to psychostimulants.

Author contributions: T.G.M.H. and T.H. designed research; J.F., S.R., F.G., A.G.M., S.K., G.A., R.A.R., J.H., and A.A. performed research; L.W., Y.Y., and G.G.K. contributed new reagents/analytic tools; J.F., S.R., F.G., A.G.M., S.K., G.A., R.A.R., J.H., K.M., G.G.K., A.A., and T.H. analyzed data; and J.F., T.G.M.H., and T.H. wrote the paper.

Reviewers: A.B., Global Institutes on Addiction; B.S., University of Fribourg; and C.T.W., Max Planck Institute of Psychiatry.

The authors declare no competing interest.

Published under the PNAS license.

[1]S.R., F.G., and A.G.M. contributed equally to this work.

[2]To whom correspondence may be addressed. Email: Tomas.Hokfelt@ki.se or tibor.harkany@ki.se.

This article contains supporting information online at https://www.pnas.org/lookup/suppl/doi:10.1073/pnas.1904006116/-/DCSupplemental.

First published December 3, 2019.

Downloaded at Palestinian Territory, occupied on November 30, 2021

www.manaraa.com

that are particularly sensitive to psychostimulants and differences between neural foci of fetal vs. maternal drug sensitivity remain ambiguous.

Here, we used immediate early gene-based mapping of transient cellular activity (15) to mark cell contingents (particularly neurons and endothelial cells) that were activated by amphetamine, nicotine, or caffeine during the period when neurogenesis peaks in the mouse prosencephalon (that is, embryonic days [E] 14 to 16) (16, 17) and reconstructed their distribution by quantitative light-sheet microscopy (18). Besides finding critical differences in the regional density of genetically tagged cell contingents, the medial preoptic area (MPN), arcuate nucleus (ARC) of the hypothalamus, and the indusium griseum (IG), all receiving dense dopamine afferentation or containing dopaminergic neurons themselves (19), emerged as invariably affected fetal brain regions. This genetic model also revealed substantial differences in brain-wide cell activation patterns between dams and their fetuses. We have then conceptually linked previous (20) and present findings on neuronal heterogeneity of the IG to show that glutamatergic neurons expressing the POU class 3 Homeobox 3 (*Pou3f3*/*Brn1*) transcription factor and many showing migratory morphology respond to amphetamine, caffeine, and nicotine at the doses used. Once arriving to their final location in the ventromedial IG, an area dominated by excitatory neurons (20), postnatal neuronal differentiation is delayed by transient intrauterine psychostimulant exposure: we identified secretagogin (*Scgn*) as a psychostimulant-sensitive molecular mark for excitatory corpus callosum (CC)-associated neurons, which exhibit bipolar morphology in both the fetal and adult IG in mice and humans. This is significant since the human IG was earlier claimed to be exclusively made up by glial cells (21). Next, we used Patch-seq to define cell type-specific marks for these regular-spiking (RS) *Scgn*$^+$ neurons, such as *Vglut1* expression. By bidirectional connectivity mapping we also showed that Scgn$^+$ IG-*Vglut1* neurons preferentially innervate γ-aminobutyric acid (GABA)-containing interneurons locally, while reciprocally connecting to one another more sporadically. Moreover, long-range IG-*Vglut1* projections link limbic to olfactory circuits. Finally, we generated *Scgn*$^{-/-}$ mice, in which IG-*Vglut1* neurons exhibited reduced intrinsic excitability. At the organismal level, the lack of Scgn triggered neuronal sensitization to methamphetamine (Meth) in the form of epileptic seizures, a major adverse condition experienced by adolescent Meth users (22, 23).

Results

Brain-Wide Activity Mapping of Prenatal Drug Exposure. Even though detailed knowledge using immediate early genes as cellular marks reflecting neuronal activation in response to psychoactive drugs exists (24–27), brain-wide and comparative activity mapping of psychostimulant drug effects in developing and adult brains has not been performed to date. Here, we induced *Fos*-CreER^{T2}::*ZsGreen1*$^{stop\text{-}floxed/stop\text{-}floxed}$ dams (15) with tamoxifen on E14.5. This was 24 h prior to administering amphetamine (10 mg/kg) (28, 29), nicotine (2 mg/kg) (11), or caffeine (6 mg/kg) (30), the most widely used psychostimulants in general (31) and during pregnancy (32), on E15.5 with 48-h survival (Fig. 1*A* and *SI Appendix*, Fig. S1*A*) to allow sufficient loading of tamoxifen-primed, drug-activated cells by ZsGreen1 (*SI Appendix*, Fig. S1 *B* and *C*). By using c-Fos histochemistry, we confirmed the efficiency and specificity of Fos-driven *Cre*-mediated recombination in the fetal cerebrum (Fig. 1*B*). Thereafter, reconstructive light-sheet microscopy for brain-wide cell activation at E17.5 (Movies S1–S4) showed that all drugs increased *ZsGreen1* expression relative to vehicle-treated controls (Fig. 1*C*). ZsGreen1 was seen in fetal and adult neurons and perivascular (endothelial) cells (*SI Appendix*, Fig. S1*D*) but neither astroglia nor micro/oligodendroglia (Fig. 1 *D* and *E*), even though a subclass of astroglia ("immediate-early astrocytes"), can express *c-Fos* in response to glutamate and inflammatory stimuli (26, 33). The preferential labeling of neurons in the fetal brain is also compatible with the late onset of astrogliogenesis, peaking neonatally, in rodents (34).

ZsGreen1$^+$ activity mapping in serial coronal sections of the fetal forebrain from saline-injected dams at E17.5 (Fig. 1*F* and *SI Appendix*, Figs. S2 and S3) revealed basal *Fos*-CreER^{T2} activity in motor and sensory cortices, hippocampus proper, and suprachiasmatic nucleus (SCN) of the hypothalamus. Considering that pacemaker systems of the SCN, including both neurons and astroglia (33, 35), can diurnally up-regulate *Fos* messenger RNA (mRNA) expression, we interpreted ZsGreen1 labeling in this hypothalamic area as an innate biological control, particularly because of the uniform (treatment-independent) size of the ZsGreen1$^+$ cell cohort (suggesting a ceiling effect due to rhythmic transcriptional activity; Fig. 1*G* and *SI Appendix*, Figs. S3 and S4). All drugs induced ZsGreen1 expression in the ventral tegmental area (*SI Appendix*, Fig. S2), which we have taken as another positive control, showing the drug-induced activation of the reward circuitry. Specifically, amphetamine increased the number of ZsGreen1$^+$ cells in cingulate, motor, and somatosensory cortices, IG (Fig. 1 *G* and *H*), tenia tecta (TT; Fig. 1*I*), striatum, hippocampus, choroid plexus, and ARC (*SI Appendix*, Fig. S3). Nicotine induced ZsGreen1 expression in cingulate, motor, and pyriform cortices, medial septum (which harbors cholinergic neurons expressing nicotinic acetylcholine receptors) (36), hippocampus, MPN, ARC, and supraoptic nucleus (*SI Appendix*, Fig. S3). Besides substantial overlap with the effects of the other dugs, caffeine triggered notable ZsGreen1 expression in the lateral diagonal band of Broca (27), MPN, and ARC (25) (Fig. 1 *F* and *G*) but not TT (Fig. 1*I*). These data demonstrate that prenatal psychostimulant exposure drives widespread and drug-specific neuronal and endothelial activation with the cingulate cortex/IG identified as a convergence point of drug action.

Next, we repeated ZsGreen1 mapping in the dams to characterize regional differences, if any, between fetal and adult brains. We found significant psychostimulant-induced cell activation in cortical, thalamic, and hypothalamic areas of which the cingulate cortex/IG and ARC invariably contained ZsGreen1$^+$ cells (*SI Appendix*, Fig. S4). Thereby, we were able to reliably capture, using heat map-based checkerboard analysis (Fig. 1*G*), regional and age-associated differences in psychostimulant sensitivity in fetal vs. adult brains.

Neuronal Targets of Psychostimulant Action in the Fetal and Adult IG. Neuroanatomical studies separate the IG from the overlying anterior cingulate cortex (ACA) in adult brain by it being negative for calbindin-D28k and, conversely, positive for Scgn or neurotrophin-3 (20, 37). Earlier studies suggest that Scgn, an EF-hand Ca^{2+}-sensor protein showing significant sequence homology to calbindin-D28k and calretinin, marks a prominent group of IG neurons whose biophysical signature resembles that of dentate granule cells (20). Therefore, Scgn is appealing as a marker of putative excitatory IG neurons. In addition, the IG receives dense monoaminergic and GABAergic innervation (38, 39). Its particularly prominent monoaminergic afferentation (*SI Appendix*, Fig. S5 *A* and *B*) that sets it apart from other cortical areas by midgestation might be a reason for its sensitivity to psychostimulant-induced perturbations.

Immunofluorescence histochemistry in combination with *Fos*-CreER^{T2}–based genetic probing suggested that ZsGreen1$^+$ neurons in the fetal IG could arise from the cortical ventricular zone: we have seen many fusiform ZsGreen1$^+$ neurons with ramifying local processes in the CC and entering the IG and lining its callosal (ventral) surface (Fig. 2*A*). At E17.5, many ZsGreen1$^+$ neurons were immunoreactive for the *Pou3f3*/*Brn1* transcription factor (Fig. 2*A*), which broadly marks glutamatergic neurons, particularly pyramidal cells destined to cortical layers 2 to 4 (40). Notably, none of the neurons

Downloaded at Palestinian Territory, occupied on November 30, 2021

www.manaraa.com

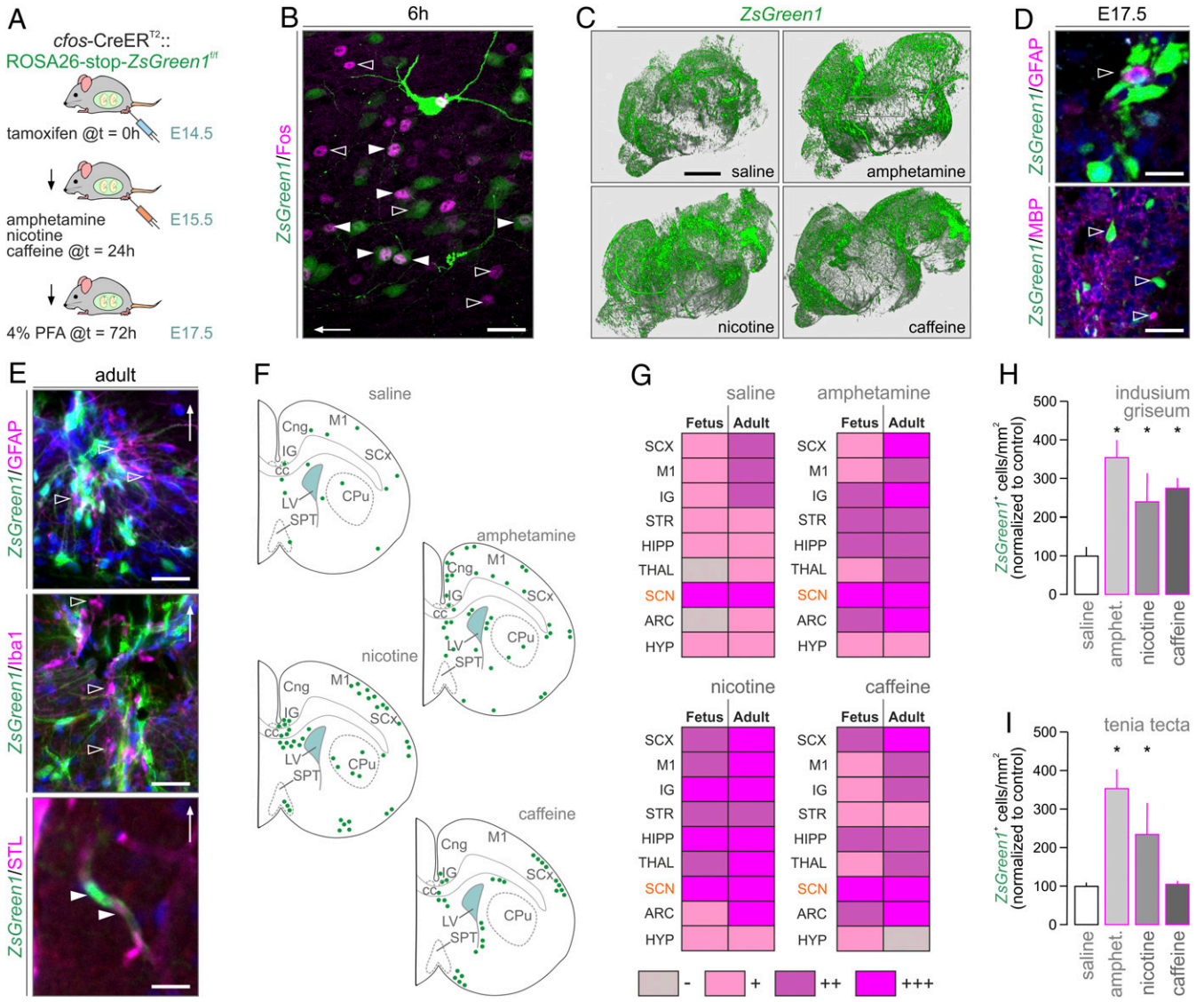

Fig. 1. Brain-wide and transgenerational cell activation maps upon psychostimulant exposure. (*A*) Experimental design in *Fos*-CreER^{T2}::*ZsGreen1*$^{stop\text{-}floxed/stop\text{-}floxed}$ dams for the correlated analysis of fetal and adult brains. (*B*) ZsGreen1$^+$ neurons label for c-Fos (solid arrowheads) 6 h after amphetamine injection. The presence of only ZsGreen1$^+$ neurons (open arrowheads) is taken as an indication of biologically relevant and transient c-Fos expression. A cortical area is shown; arrow indicates the pial surface. (*C*) Three-dimensional rendering of optically cleared fetal ZsGreen1$^+$ brains after psychostimulant exposure. Neither fetal (*D*) nor adult (*E*) brains showed ZsGreen1 signal in astroglia (GFAP$^+$), microglia (Iba1$^+$), or oligodendrocyte-like (MBP$^+$) cells (open arrowheads). Endothelial cells (arrowheads) were visualized using *Solanum tuberosum* lectin (STL). In *E*, the IG is shown with arrows pointing dorsally. (*F*) Cellular ZsGreen1$^+$distribution in coronal sections spanning the IG. For abbreviations and consecutive levels see *SI Appendix*, Fig. S3. (*G*) Comparison of cell activation patterns between fetuses and their respective dams (Adult). The SCN with its periodic *Fos* expression served as positive control. (*H* and *I*) Quantitative increases in ZsGreen1$^+$ cell numbers in select brain areas upon psychostimulant treatment. Data were acquired using Arivis after light-sheet microscopy (*C*, *H*, and *I*). Data were expressed as percentages of control, and are shown as means ± SEM; $*P < 0.05$ (Student's *t* test). (Scale bars: 1.5 mm [*C*], 30 μm [*D*, *Lower*], 20 μm [*B* and *E*], 10 μm [*D*, *Upper*].)

populating the prospective IG expressed Scgn at E17.5, irrespective of them being eventually ZsGreen1$^+$. This unexpected feature distinguishes the IG from other forebrain areas in which Scgn expression usually precedes that of other neuron-specific Ca^{2+}-binding proteins (20). The lack of Scgn together with preferential D1 dopamine receptor expression (*SI Appendix*, Fig. S5*A*) in CC-associated glutamatergic neurons could explain, at least in part, their preferential psychostimulant sensitivity in the fetal IG. This hypothesis is also supported by the finding that in the adult brain ZsGreen1$^+$ neurons in the IG are small to medium-sized in diameter, multipolar, Scgn$^-$, and positioned relatively distant from the pial surface (Fig. 2*B*). These cellular features suggest nonexcitatory identity. The fact that Scgn$^+$ glutamatergic neurons were invariably ZsGreen1$^-$ in the IG of the dams corroborates earlier observations on neuroprotection mediated by Ca^{2+}-binding and sensor proteins (41–46). Scgn/ZsGreen1 coexistence in the ARC served as positive (biological) control (Fig. 2*B* and *SI Appendix*, Fig. S1 *D* and *E*), which is compatible with their expression of nicotinic acetylcholine receptors and cocaine and amphetamine-regulated transcripts (47). Here, we have specifically mapped the developmental trajectory and psychostimulant sensitivity of Scgn$^+$ excitatory IG neurons.

First, we find Scgn be gradually enriched in the IG from postnatal day (P) 12 and reaching adult levels by P25 (Fig. 2*C*). Likewise, neuropeptide Y expression was transient in IG and detectable only on P5 (*SI Appendix*, Fig. S5 *B–D*). These observations suggest that excitatory neuron development is a

Downloaded at Palestinian Territory, occupied on November 30, 2021
www.manaraa.com

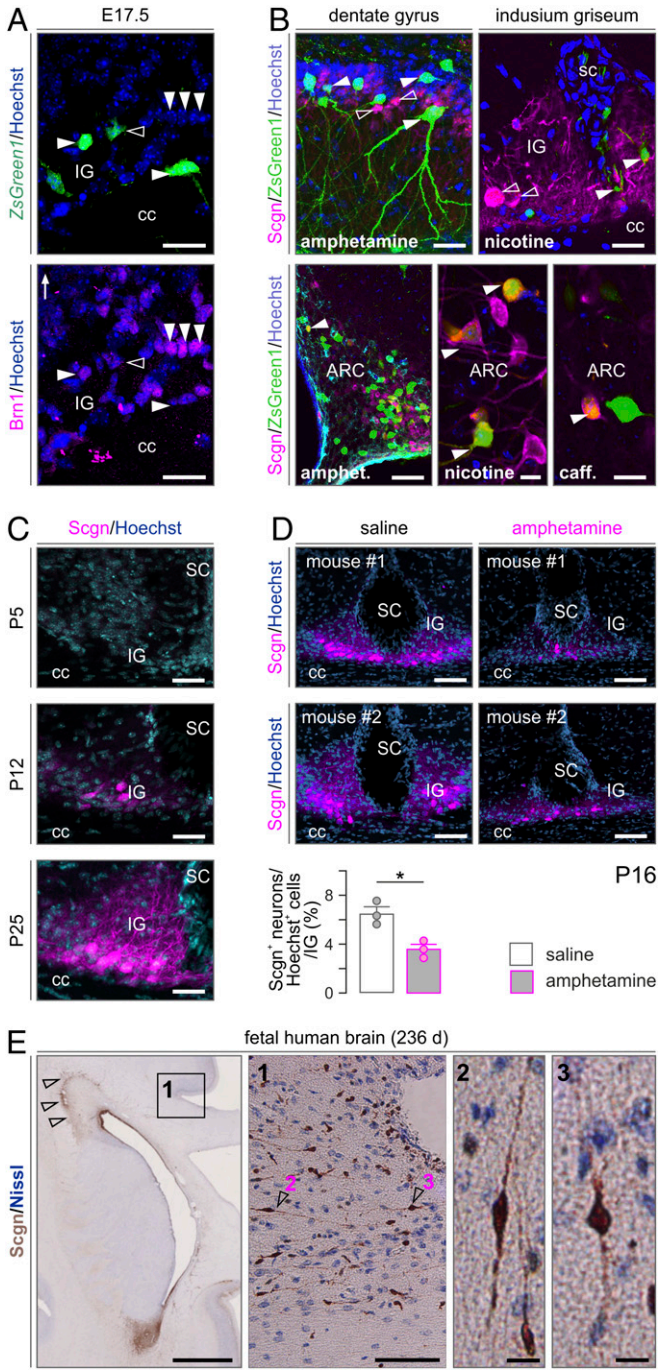

Fig. 2. Psychostimulant sensitivity and ontogeny of *Scgn*$^+$ neurons in the IG. (*A*) At E17.5, many psychostimulant-responder neurons in the IG express *Pou3f3*/*Brn1* (arrowheads; open arrowhead shows the lack of colocalization), a transcription factor for cortical pyramidal cells (40), and coincidently lack Scgn. (*B*) In contrast, in the adult DG, IG and AHC (*Top*), psychostimulant-induced ZsGreen1 expression (solid arrowheads) did not label Scgn$^+$ neurons (open arrowheads). However, Scgn$^+$ neurons of the ARC showed coincident ZsGreen1 expression (solid arrowheads). (*C*) Scgn localization in the mouse IG during postnatal development with P12 taken as the earliest time point at which Scgn was successfully detected. (*D*) Prenatal amphetamine exposure significantly reduces Scgn expression in the IG on P16. Data were expressed as means ± SEM from $n = 3$ per treatment; $^*P < 0.05$. (*E*) Scgn$^+$ neurons line the IG in the human fetal brain. Left to right: Coronal section of a 236-d-old human fetal brain at the level of the anterior horn of the lateral ventricle. Arrowheads indicate Scgn expression in the rostral migratory stream. Open rectangle denotes the position of high-magnification inset 1 on the dorsal surface of the genu/truncus corporis callosi. Arrowheads identify the position of Scgn$^+$ neurons shown at high resolution; 2 and 3: Scgn$^+$ neuroblasts in the lateral part of the IG. caff., caffeine; sc, sulcus centralis. (Scale bars: 1 cm [*A*], 120 μm [*B*, *Bottom Left* and *D*], 50 μm [*B*, *Top Left*], 30 μm [*A* and *B*, *Top Right* and *C*], and 12 μm [*B*, *Bottom Middle* and *Right and E*, 1 and 2].)

protracted process in the IG, likely limiting the excitability of this neuronal contingent during fetal development. Next, we argued that intrauterine psychostimulant exposure might perturb *Scgn* gene expression in IG neurons if Scgn itself is a critical and activity-dependent differentiation mark. To test this hypothesis, we have treated pregnant mice with amphetamine (10 mg/kg) as above and sampled their male offspring on P16, a time point when Scgn level is substantial yet submaximal (Fig. 2*D*). As such, prenatal amphetamine application resulted in a significantly delayed Scgn expression in the IG (Fig. 2*D*). These data directly link *Scgn* expression to psychostimulant sensitivity in excitatory neuronal progenies of the developing IG.

Considering that neither cellular nor detailed network features of Scgn$^+$ IG neurons are known [beyond some rudimentary biophysical characteristics (20)], we have molecularly characterized Scgn$^+$ IG neurons using the Patch-seq workflow (48). Subsequently, we addressed if genetic ablation of Scgn increases neuronal sensitivity to Meth.

Scgn Marks both the Mouse and Human IG. The supracallosal domain of the IG resides in 2 parallel narrow stripes of gray matter situated rostrocaudally on the dorsal surface of the CC (Fig. 3 *A* and *B*). Once stretching over the genu of the CC, a small descending dorsoventral line of IG neurons forms the anterior hippocampal continuation (AHC) (Fig. 3*B*). Earlier, we have shown that Scgn marks the IG and AHC, which share most microanatomical characteristics, in both lower primates and rodents (20). These data are recapitulated here (Fig. 3 *A*–*F*) with an alternative antibody (*Materials and Methods* and *SI Appendix*, Fig. S5*F*) and extended by CUBIC (clear, unobstructed brain imaging cocktails and computational analysis)-based tissue clearing and intact tissue imaging to show that Scgn also labels the axonal bundles emanating from the IG and AHC and turning under the genu of the CC (Fig. 3*G*). Moreover, our localization of Scgn$^+$ neurons in the pyramidal layer of the CA1 and CA2 subfields of the mouse hippocampus (Fig. 3*C*), as well as the dentate gyrus (DG) and fasciola cinerea (FC), visualizing the extrahippocampal formation (Fig. 3*C*), reconciles data from postmortem human hippocampal CA1, where Scgn was implicated in conferring resistance to neurodegeneration (49).

While the rodent and primate IG are known to contain neurons (20), the cellular organization of the human IG is considered different with glial cells recognized as its building blocks (21). This notion prevails despite the fact that, at the gross anatomy level, the IG in humans is reminiscent of its mouse equivalent by being adherent to the lamina terminalis and extending between the genu and splenium of the CC. When using Scgn as a molecular marker (Fig. 3 *H* and *I*), we find bipolar neuron-like cells with fusiform perikarya and long processes in both the fetal (third trimester; Fig. 2*E*) and adult human IG (Fig. 3 *H* and *I*). The neuronal identity of these cells is supported by their expression of either calretinin (Fig. 3*H*) or microtubule-associated protein 2 (MAP2; Fig. 3*I*), even though these markers seem abundant in nonoverlapping cell cohorts. Thus, we suggest that Scgn$^+$ neurons with morphological features reminiscent of relay or dormant migratory neurons earlier found in the olfactory tubercle of humans (45) also exist in the human IG.

Long-Range Connectivity of Scgn$^+$ FC/IG Neurons. The extrahippocampal pathway with its continuum of Scgn$^+$ neurons is a complex integration loop caudally exiting the hippocampus through the subiculum toward the FC. To map if long-range connections

Downloaded at Palestinian Territory, occupied on November 30, 2021

www.manaraa.com

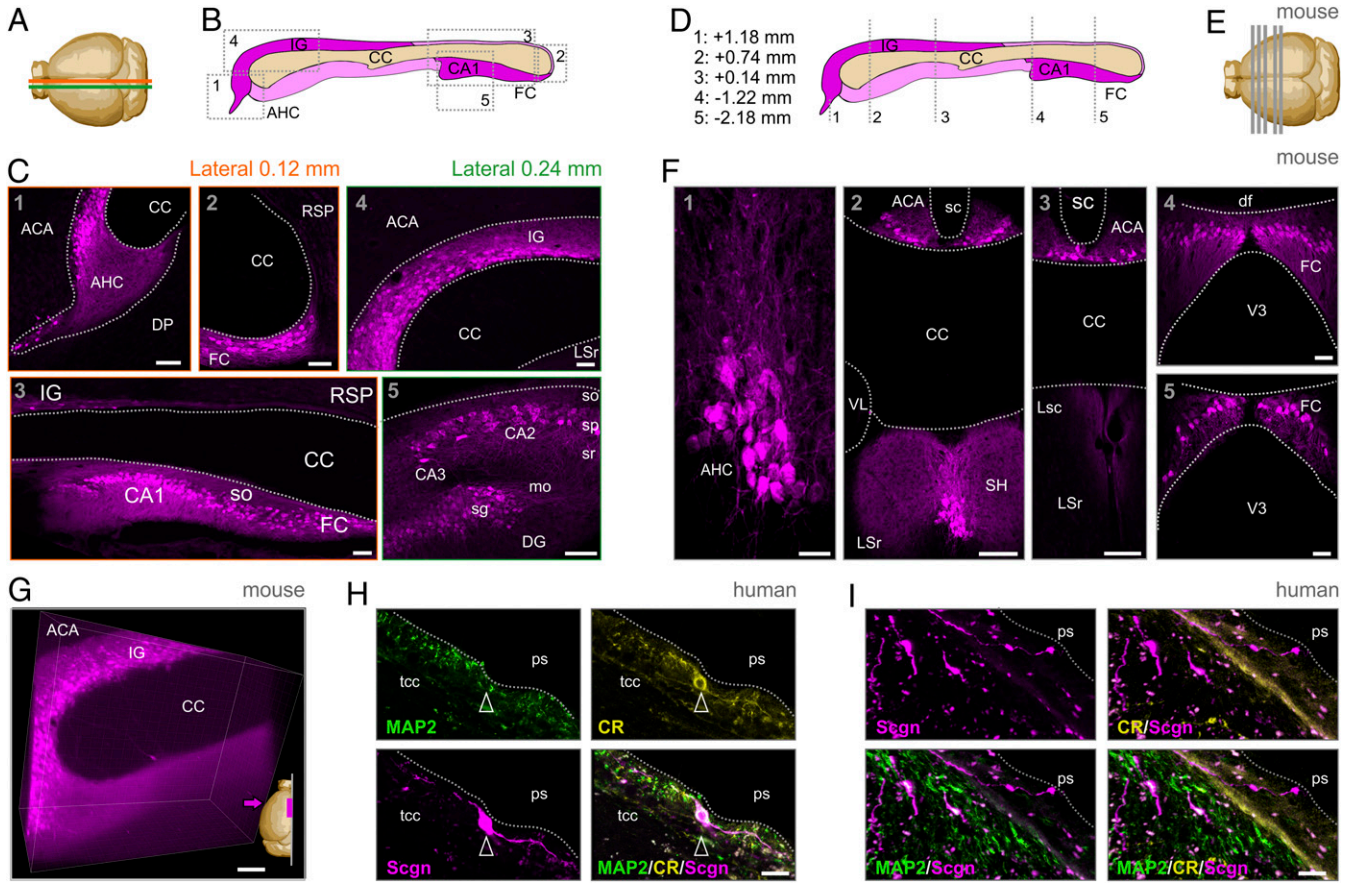

Fig. 3. Anatomy of the mouse and human IG. (*A*) Brain scheme with orange and green lines indicating the cutting planes at 0.12 mm and 0.24 mm from the midline. (*B*) Sagittal scheme of the mouse extrahippocampal formation, including IG. Gray dashed rectangles indicate the location of panels in *C*. (*C*) Scgn immunoreactivity (magenta) in the anatomical regions of the extrahippocampal formation defined by the Allen Brain Atlas. (*D*) Coronal scheme of the mouse extrahippocampal formation. Gray dashed lines (equally spaced for illustration) and coordinates relative to bregma indicate the coronal cutting planes shown in *E*. (*E*) Brain scheme with coronal planes of tissue sampling. (*F*) Scgn immunoreactivity at the anterior–posterior coordinates indicated. (*G*) Three-dimensional image of optically cleared IG with Scgn immunostaining. A 500-μm sagittal block is shown. Magenta arrow indicates the point of view. (*H*) Human IG with a $Scgn^+$ IG neuron close to the pial surface (ps) expressing calretinin (CR) but not MAP2. (*I*) $Scgn^+/CR^-$ bipolar neurons (arrowheads) in human IG. Both $Scgn^+/MAP2^+$ and $Scgn^+/MAP2^-$ neurons could be found. CA1-3, cornu ammonis 1 to 3 subfields; df, dorsal fornix; DP, dorsal peduncular cortex; LSc/r, lateral septal nucleus caudal/rostroventral; mo, straum moleculare; RSP, retrospinal area (ventral); sc, sulcus centralis; SH, septohippocampal nucleus; sg, stratum granulosum; so, straum oriens; sp, stratum pyramidale; sr, stratum radiatum; tcc, truncus corporis callosi; VL, lateral ventricle; V3, third ventricle. (Scale bars: 100 μm [*F*, 2 through 4], 50 μm [*C*, 1 through 5, *E*, and *F*, 4, and *G*], 20 μm [*F*, 1 and 5], and 10 μm [*H* and *E*].)

exist between the FC and IG, biotinylated dextran amine (BDA) was injected into the FC and used to anterogradely trace FC efferents (*SI Appendix*, Fig. S6*A*). BDA^+ axons traveled around the splenium of the CC and split into parallel tracts at its ventral and dorsal surfaces (*SI Appendix*, Fig. S6*B*). BDA^+ axons either terminated on the dendrites of $Scgn^+$ IG neurons (*SI Appendix*, Fig. S6 *C* and *D*) or eventually ran parallel with those (*SI Appendix*, Fig. S6*E*). Next, we tested if $Scgn^+$ neurons receive synaptic inputs from the olfactory bulb, an experiment prompted by the notion that $Scgn^+$ neurons also line the rostral migratory stream (as "shell cells") (45) and populate the olfactory bulb. Here, cholera toxin B was used as retrograde tracer and injected into the main olfactory bulb. Indeed, populations of $Scgn^+$ neurons along the IG were seen colabeled for cholera toxin B and Scgn (*SI Appendix*, Fig. S6*F*). These anatomical features suggest that $Scgn^+$ neurons can relay information along the FC–IG–olfactory bulb circuit (Fig. 4*A*).

Synaptic Inputs to and Local Circuits of $Scgn^+$ IG Neurons. Neuronal computation in the IG summates the activity of subcortical cholinergic and midbrain monoaminergic territories, which is supported by the accumulation of afferent inputs harboring choline acetyltransferase, dopamine β-hydroxilase, tyrosine hydroxylase (TH), D2 dopamine receptors (*SI Appendix*, Fig. S5*B*), or 5-HT receptors ($5\text{-}HTR_7$) (38, 39). This anatomical complexity suggests that IG neurons might read out source network information for feedback to the hippocampus. The diversity of inputs is testable by, for example, histochemistry given the dichotomy of vesicular glutamate transporters (VGLUTs), with VGLUT1 and VGLUT2 segregating to cortical and thalamic sources (Fig. 4*B*), respectively (50, 51). We find $VGLUT1^+$ or $VGLUT2^+$ synaptic terminals on $Scgn^+$ IG neurons organized by a strict topography (Fig. 4 *C* and *D*), with $VGLUT1^+$ boutons targeting dendritic compartments, whereas $VGLUT2^+$ terminals arrive to neuronal somata (Fig. 4 *C* and *D*). $VGLUT3^+$ terminals were found scattered along the somatodendritic axis (Fig. 4*D*). GABAergic interneurons populate the dorsolateral domain of the IG (Fig. 4 *C* and *E*) and are recruited to local circuits. The lack of colocalization between Scgn and GFP in $GAD67^{gfp/+}$ mice in intact, CUBIC-cleared tissues (52) reinforces that large-diameter $Scgn^+$ IG neurons are non-GABAergic (Fig. 4*E*) and instead are entrained by local GABA sources.

Besides their macrocircuit constellation, little is known about the local microcircuitry in which $Scgn^+$ IG neurons are embedded. Hence, we probed local connectivity using triple whole-cell

Downloaded at Palestinian Territory, occupied on November 30, 2021
www.manaraa.com

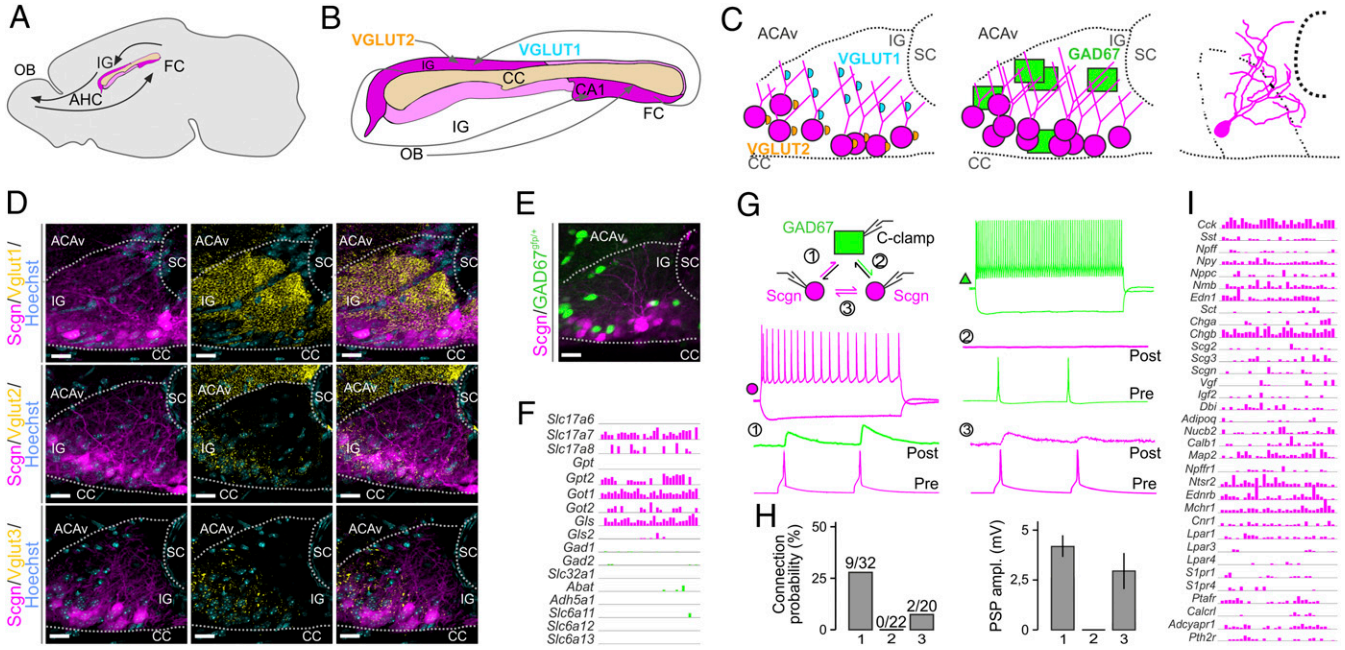

Fig. 4. Local networks in the IG. (*A*) Sagittal scheme of the mouse extrahippocampal formation with the CC and IG and putative connectivity between the olfactory bulb (OB) and FC indicated. (*B*) Predicted glutamatergic connections, including the integration of excitatory afferents containing VGLUT1 and VGLUT2. (*C*) Coronal scheme of the IG with the cellular positions of VGLUT1$^+$ and VGLUT2$^+$ synaptic puncta (*Left*), the location of excitatory Scgn$^+$ vs. GAD67$^{gfp/+}$ GABAergic neurons (*Middle*), and reconstruction of a biocytin-filled Scgn$^+$ neuron (*Right*). (*D*) Distribution of VGLUT1, VGLUT2, and VGLUT3 in the IG. Note the predominance of VGLUT1$^+$ innervation. Sections were at the level of +0.6 mm from bregma. (*E*) Spatial distribution of excitatory Scgn$^+$ and GAD67$^{gfp/+}$ GABAergic neurons in IG. (*F*) Expression of neurotransmitter modality-related genes identified with Patch-seq. Log_2 expression of genes coding for glutamatergic (magenta) and GABAergic (green) neurotransmitter synthesis, vesicular loading, and degradation. Numbers indicate possible connected neurons. (*G*, *Top Left*) Setting of ex vivo triple whole-cell electrophysiology recordings. (*G*, *Middle*) Representative firing patterns of Scgn$^+$ (magenta) and GAD67$^{gfp/+}$ (green) neurons (*G*, *Top*), with rheobasic spikes in gray; 1, 2, and 3 show combinations of possible connections with representative examples of paired recordings. (*H*) Bar graphs depict the connection probability (*Left*) and amplitudes of recorded postsynaptic potentials (PSPs) (*Right*). Data were expressed as means ± SEM. (*I*) Neuropeptide and neuropeptide receptor gene expression in IG neurons, revealed by Patch-seq. ACAv, anterior cingulate area (ventral); AHC, anterior hippocampal extension; CA1, cornu ammonis subfiled 1; sc, sulcus centralis. (Scale bars: 15 μm [*D*], and 20 μm [*E*].)

patch-clamp recordings in GAD67$^{gfp/+}$ mice (Fig. 4*G* and *SI Appendix*, Fig. S7), where we visually distinguished fast-spiking (FS) GABA interneurons and GFP$^-$ IG neurons, the latter being RS (Fig. 4*G*). We used triplets consisting of 1 GAD67$^{gfp/+}$ and 2 GFP$^-$/RS IG neurons to test if excitatory IG neurons (post hoc identified as Scgn$^+$) are densely interconnected for local amplification and summation of neural information. We used the electrophysiological profile described by Mulder et al. (20) to identify Scgn$^+$ neurons. This setting was also advantageous to assess reciprocal connectivity of Scgn$^-$/FS and RS IG neurons (tested 72 putative connections; Fig. 4 *G* and *H*). We found ∼27% connection probability from RS-to-FS neurons (9 out of 32 tested; Fig. 4*H*) with an average amplitude of 4.1 ± 0.7 mV. Reciprocal connections between FS-and-RS neurons were not found. Determination of Scgn$^+$ IG neuron interconnectivity revealed the presence of excitatory connections in ∼10% of the cases (2 out of 20; Fig. 4*H*), with an amplitude of 2.7 ± 1.1 mV. Thereby, we hypothesize that activation of the excitatory component of the IG is primarily achieved by cortical and subcortical synaptic inputs (38, 39) rather than through self-amplification loops locally.

Patch-seq Profiling of Scgn$^+$ Neurons. The only existing dataset on Scgn$^+$ neurons posits similarities between DG and IG neurons on the basis of biophysical similarities, which is compatible with a broader view of the IG being an anterior extension of the DG (53). However, molecular analysis is required for this hypothesis to stand. Therefore, we have fed RNA samples from all neurons that had undergone electrophysiological recordings into our Patch-seq workflow (48) to achieve precise gene expression profiling (Fig. 4 *F* and *I* and *SI Appendix*, Fig. S8).

The analysis of genes associated with inhibitory or excitatory neurotransmission in RNA aspirates of IG neurons revealed the predominance of glutamate-synthetizing and -degrading enzymes (Fig. 4*F*). In contrast, the enzymatic machinery for GABA synthesis (e.g., *Gad1* and *Gad2*) was not expressed (detection threshold = >2 counts in >5/30 IG neurons) (Fig. 4*F*). To use precise molecular mapping to predict (and support) how IG neurons are synaptically wired in the IG, we extracted single-cell RNA-sequencing (RNA-seq) data for neuropeptides and receptors (Fig. 4*I*). We find *Scgn* as a marker gene at low transcript levels, an observation compatible with its slow protein turnover (54). Therefore, homogeneity of the electrophysiological signatures and molecular parameters of non-GAD67$^{gfp/+}$ IG neurons was used as cellular classifier (Fig. 4*I*). Excitatory IG neurons expressed endothelin receptor type B (*Ednrb*), neurotensin receptor 2 (*Ntsr2*), melanin-concentrating hormone receptor 1 (*Mchr1*), cannabinoid receptor 1 (*Cnr1*), and parathyroid hormone receptor 2 (*Pthr2*), indicating the physiological role of these neurons in distinct hormonal responses, particularly embedding IG neurons into hormonal feedback networks. In addition, mRNA transcripts for many classical and other neuropeptides were also seen, including cholecystokinin (*Cck*), somatostatin (*Sst*), neuropeptide FF (*Npff*), neuropeptide Y (*Npy*), natriuretic peptide C (*Npcc*), neuromedin B (*Nmb*), chromogranin B/secretogranin B (*Chgb*), and calbindin D28k (*Calb1* at detection threshold = >2 counts in >5/30 IG neurons; Fig. 4*I*).

Even though mRNA expression is taken broadly to be indicative of neuronal identity, mRNA-to-protein translation does not necessarily occur, which can bias the biological interpretation of single-cell RNA-seq data. Here, we show that despite the presence of *Npy*

Downloaded at Palestinian Territory, occupied on November 30, 2021

www.manaraa.com

mRNA in all of the Patch-Seq–recorded neurons, neuropeptide Y (NPY) immunoreactivity was not detectable in adult IG. Instead, we find NPY-expressing neurons at P5 (*SI Appendix*, Fig. S5*C*), indicating a putative and transient developmental role for NPY, equivalent to other neuropeptides in the neonatal period (55). Similarly, the presence of *Cck* mRNAs in IG was reported in our earlier work on a $CCK^{BAC/DsRed}$::$GAD67^{gfp/+}$ composite mouse line (18, 48), even though conventional histochemistry fails to visualize CCK protein. Furthermore, lower levels of *Drd1* mRNA were also detected and confirmed by genetic labeling in the corresponding D1R-GFP mouse line (*SI Appendix*, Fig. S5*A*).

Finally, we aimed to identify cell type-specific markers of excitatory IG neurons by using a contrast analysis between our dataset and cortical single-cell RNA-seq data (56). We filtered the set of cortical genes with zero or low expression [low-pass-filtered by the interquartile range of expression values, i.e., lowest 25% of the expressed genes identified by Tasic et al. (56)] and compared these to highly expressed genes in IG from our Patch-seq dataset (high-pass-filtered to extract the highest 25% of expressed genes). This intersectional analysis returned interleukin-16 (*Il-16*), aggrecan (*Acan*), FERM domain-containing protein 2 (*Frmpd1*), hepatocyte growth factor (*Hgf*), and Ca^{2+}-binding protein-7 (*Cabp7*) as preferentially expressed in excitatory IG neurons (vs. cortical ones; *SI Appendix*, Fig. S8*B*). Interestingly, we found neither *Prox1* nor *Prox2* expression, which identify both fetal and adult dentate granule cells (57), thus suggesting the molecular demarcation of IG neurons at least at specific segments of their transcriptional control. These data establish the precise molecular makeup of excitatory IG neurons, set them apart from their cortical counterparts, and allow testing of both neuronal connectivity and hormone signaling.

Adult *Scgn*$^{-/-}$ Mice Are Sensitive to Meth. Meth, a derivate of amphetamine, is known to obstruct neuronal excitability (58, 59). Therefore, we first confirmed that acute superfusion of Meth (50 μM) directly affects RS IG neuron excitability during ex vivo whole-cell current clamp recordings. Indeed, Meth suppressed action potential (AP) formation in IG neurons, leading to a maximum of a single AP on a stimulus step (Fig. 5*A*), which showed a smaller amplitude and significantly increased half-width (Fig. 5*B*). The Meth effect was instantaneous, robust, and reversible (*SI Appendix*, Fig. S9*A*) and also occurred in *Scgn*$^{-/-}$ slices (*SI Appendix*, Fig. S9*B*).

High-dose or repeated Meth administration triggers extensive neuronal apoptosis and astrogliosis in the IG in vivo (28, 29, 60). As a behavioral effect downstream, Meth can either trigger epileptic seizure-like activity (23, 61, 62) or enhance those that preexisted. Given the insensitivity of *Scgn*$^{+}$ limbic (including IG) neurons to psychostimulants, we asked if genetic deletion of this Ca^{2+} sensor would alter the sensitivity of the IG circuit to Meth, demonstrated by increased seizure activity. This hypothesis rests on the knowledge that the loss of other Ca^{2+} sensors and buffers perturbs neuronal excitability (44, 63, 64). Here, we injected both wild-type ($n = 10$) and *Scgn*$^{-/-}$ mice ($n = 11$) with Meth (15 mg/kg, intraperitoneally, 3 times at 90-min intervals; Fig. 5*C*) and scored animal behavior by the SHIRPA protocol (65, 66) 60 min after each Meth cycle (T1 through T3; Fig. 5 *C* and *E*). Among the parameters scored, gait, tremor, licking behavior, and clonic convulsions were significantly different between the genotypes, and *Scgn*$^{-/-}$ mice showed significantly worsened signs toward Meth acutely (Fig. 5*E*). Clonic convulsions in *Scgn*$^{-/-}$ mice at T2 were particularly notable (Fig. 5*D*). *Scgn*$^{-/-}$ mice (54, 67) also produced more severe symptoms as fragmented locomotion and increased wall/floor licking, which often coincided with continuous reversing (Fig. 5*E* and Movies S5 and S6). These data show that *Scgn* gene ablation increases Meth vulnerability.

Next, we asked if *Scgn* is critical in determining pathophysiological changes in the biophysical characteristics of IG neurons by comparative analysis of wild-type vs. *Scgn*$^{-/-}$ mice (54, 67) using whole-cell patch-clamp recordings. For wild-type IG neurons, we have identified the rheobasic AP threshold (AP_{thr}) by applying 1- to 2-pA incrementing current steps. All cells showed a prepotential when reaching the AP_{thr} and continued spiking thereafter (Fig. 5 *F*, *Top*). Herein, an after-depolarization phase following a fast after-hyperpolarization phase was sufficient to evoke a second AP immediately after the first rheobasic AP (Fig. 5 *F*, *Middle*). In contrast, *Scgn*$^{-/-}$ neurons did not produce a prepotential along with a reduced number of APs on their rheobasic responses (Fig. 5*F* and *SI Appendix*, Fig. S10). Their after-depolarization amplitudes were also significantly reduced. In sum, quantification of all AP parameters and firing patterns revealed significant differences between wild-type ($n = 19$) and *Scgn*$^{-/-}$ ($n = 21$) RS IG neurons in, for example, resting membrane potential (V_{rest}), number of APs on the rheobasic step, and double-threshold firing frequency (2× freq) (Fig. 5 *F*, *Bottom*).

Finally, we sought to determine if in vivo Meth administration differentially affects the excitability of IG neurons in wild-type vs. *Scgn*$^{-/-}$ mice. To this end, we performed patch-clamp recordings in ex vivo brain slices 24 h after behavioral testing (Fig. 5*C*). A history of Meth exposure significantly lowered the firing rate on rheobasic responses (to levels similar to those in *Scgn*$^{-/-}$ neurons at baseline) and eliminated the after-depolarization in wild-type IG neurons (Fig. 5*G*). In turn, *Scgn*$^{-/-}$ IG neurons expressed a bursting rheobasic response (yet no change in frequency) 24 h after Meth exposure, which appeared with considerable time lag upon rheobasic stimuli (Fig. 5*G*). Post hoc morphological reconstruction confirmed that the same subtype of RS neurons at comparable locations in the ventromedial IG were probed (*SI Appendix*, Fig. S10). Their lesser Meth responses upon Scgn knockout (*SI Appendix*, Fig. S11) define the biophysical footprint of Meth administration. Thus, Meth is identified as a psychostimulant that retunes basic biophysical properties (e.g., V_{rest}) and capacity to fire AP trains in a *Scgn*-dependent manner (Fig. 5*G*). Cumulatively, these data provide a sufficiently broad set of indications to suggest that *Scgn* ablation compromises IG neurons in their level of excitability and sensitizes them to Meth-induced maladaptation, which might be relevant to scaling psychostimulant sensitivity along the DG→FC→IG→olfactory circuit.

Discussion

Parcellation of cortical areas through the correlated molecular, cellular, and circuit-level interrogation of their (primarily neuronal) constituents revolutionized modern neurobiology by distinguishing a kaleidoscope of cellular subtypes [or modalities (68, 69)]. However, studies which assign select neuronal contingents as function determinants to brain-state changes upon environmental stimuli (irrespective of these being adverse or benign) are at their infancy. Here, we combined psychostimulant-induced brain-wide genetic activity mapping (15) with Patch-seq interrogation of neurons (48) to capitalize on the advantages of the most powerful neuronal phenotyping techniques available to date. Our studies pinpoint the IG as the limbic area containing neurons ultimately activated by amphetamine (or Meth), nicotine, and caffeine. A plausible reason for such sensitivity is the unique developmental trajectory, molecular/neurochemical identity, and circuit complexity of excitatory IG neurons, including the late postnatal expression of Scgn, a Ca^{2+}-sensor protein. Moreover, the IG receives dense innervation from monoaminergic and cholinergic subcortical afferents (38, 39), which we view as a molecular underpinning for its selective sensitivity to psychostimulants. The neurochemical complexity of long-range afferentation together with the hierarchical distribution of glutamatergic afferents along the somatodendritic axis of excitatory IG neurons produces a strict organizational layout for the integration of synaptic inputs from cortical/hippocampal ($VGLUT1^{+}$; arriving to dendrites),

Downloaded at Palestinian Territory, occupied on November 30, 2021
www.manaraa.com

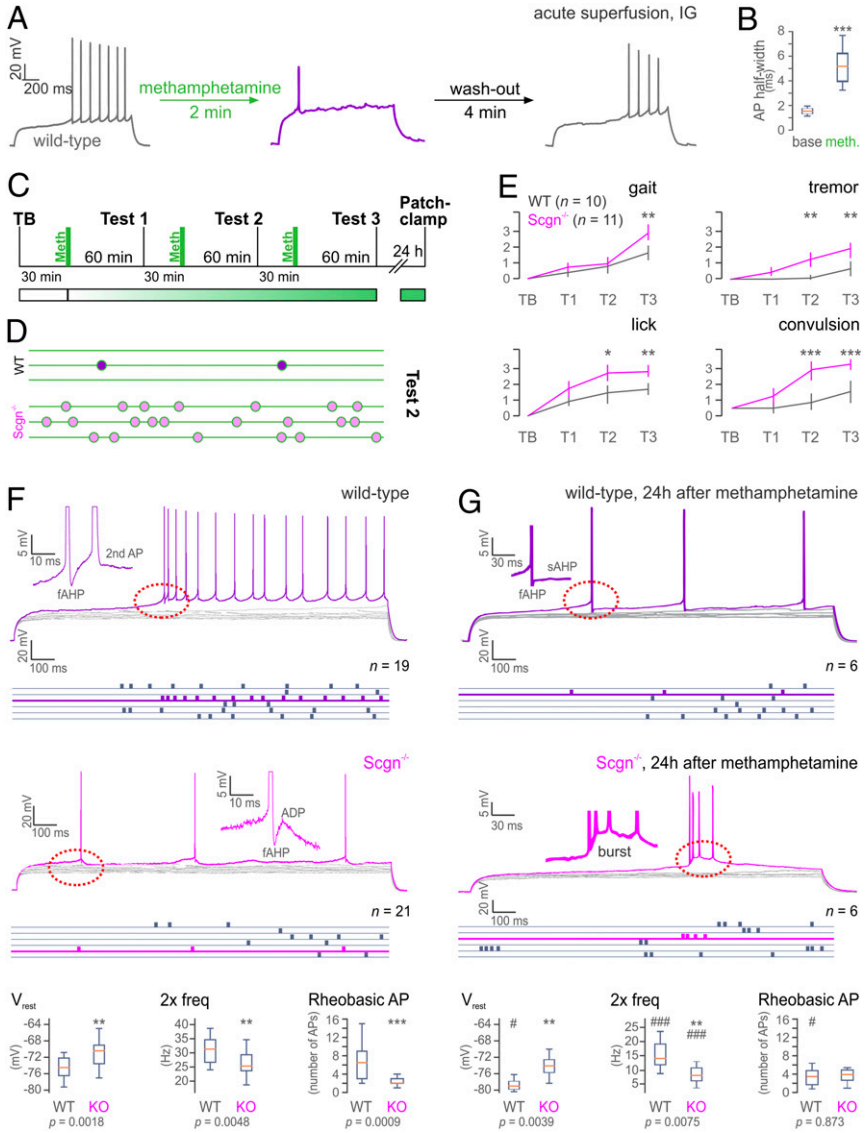

Fig. 5. Scgn ablation sensitizes to Meth. (*A*) Meth superfusion acutely inhibits AP discharges in IG neurons in wild-type (WT) mice ($n = 2/n = 4$). (*B*) Significant AP half-width increase during bath application of Meth. (*C*) Experimental design of Meth administration, behavioral testing, and ex vivo electrophysiology. (*D*) Convulsions in WT vs. *Scgn*$^{-/-}$ mice during test 2 (green lines represent 60 s). (*E*) Summary of behavioral scores (gait, tremor, lick, and convulsion) in TB and T1 through T3 of Meth-injected WT ($n = 10$) and *Scgn*$^{-/-}$ mice ($n = 11$). Data were evaluated by 2-way ANOVA using a repeated-measures design [gait: $F_{time} = 39.26$, $F_{genotype} = 14{,}13$; tremor: $F_{time} = 30{,}09$, $F_{genotype} = 60{,}45$; lick: $F_{time} = 56.93$, $F_{genotype} = 71.12$; convulsion: $F_{time} = 77.86$, $F_{genotype} = 165.24$; dF = (1, 19), in all cases $P < 0.001$]. Post hoc (group) comparisons are shown. (*F*) Excitability and intrinsic discharge properties of IG neurons from WT ($n = 7/n = 19$) and *Scgn*$^{-/-}$ mice ($n = 7/n = 21$). Rheobasic responses in purple (WT) and pink (*Scgn*$^{-/-}$) with raster plots showing firing rates in blue. Note the reduced firing rate, and the lack of a prepotential (red dashed circle) in *Scgn*$^{-/-}$ IG neurons (insets show after-depolarization [ADP] kinetics). Comparison of biophysical parameters from WT vs. *Scgn*$^{-/-}$ neurons (*Bottom*). (*G*) Excitability and intrinsic properties of IG neurons from WT ($n = 4/n = 6$) and *Scgn*$^{-/-}$ mice ($n = 3/n = 6$) 24 h after Meth exposure. Note the reduced firing rate and decreased ADP in WT, as well as bursting in *Scgn*$^{-/-}$ IG neurons (red dashed circles). (*Bottom*) Comparison of intrinsic parameters from WT vs. *Scgn*$^{-/-}$ neurons 24 h after Meth exposure and their statistical comparison to naive state measures (*F*; labeled with #). Data were expressed as means ± SEM (whisker plots show minimum-to-maximum distribution). $^{*/\#}P < 0.05$, $^{**/\#}P < 0.01$, $^{***/\#\#\#}P < 0.001$; 2-sample *t* test. TB, test at baseline; T1 through T3, tests 1 through 3; 2× freq, firing frequency at 2× rheobase stimulation.

subcortical/olfactory (VGLUT2$^+$; arriving to somata), and midbrain monoaminergic inputs (VGLUT3$^+$, TH$^+$/DAT$^+$ targeting perisomatic domains).

By textbook definition, the IG is referred to as a glia-laden area. This view is in part supported by developmental biology data from rodents and humans associating the IG with callosal development, which relies on glia-derived guidance cues (34, 70, 71): Pioneer axons of the CC are spatially organized by the IG and the glial wedge dorsally, with the subcallosal sling positioned ventrally (72). This opinion is further strengthened by the cellular anatomy of the human IG, which is perceived as a glial plate (21), probably due to the lack of neuronal markers, particularly those helpful to visualize fine neuronal morphology. The "glial dominance hypothesis" persists despite detailed knowledge on the existence of immature neurons in the IG at birth, which reach mature neuronal morphology by P15 in rodents (including receptor expression) (70, 71).

Notably, the subcallosal sling was recently redefined as a neuron-enriched territory (72). Likewise, we make an effort to reclassify the IG as a neuronal domain given the existence of functionally specialized and CC-associated glutamatergic neurons to reside ventrally, while GABA cell populations accumulate dorsolaterally. By relying on Scgn and neuropeptides, we

Downloaded at Palestinian Territory, occupied on November 30, 2021

www.manaraa.com

show that excitatory IG neurons are immature at P5 and become neurochemically specialized by P12 to P16, by which time Scgn immunolocalization fully resolves the principal circuit design of both the IG and AHC. In fact, Scgn alone is sufficient to outline a DG→FC→IG→olfactory bulb loop, in which tract tracing distinguishes FC neurons to project to the IG that, in turn, innervate the olfactory bulb. Morphologically, $Scgn^+$ IG neurons in rodent and human brains are similar, with uniquely long processes running parallel with the callosal surface. Our data on the existence of Scgn-only vs. $Scgn^+$/calretinin$^+$ neuronal subsets suggest essential heterogeneity or the activity-dependent regulation of Scgn (or calretinin) expression in human IG neurons. However, the use of Patch-seq itself carries sufficient precision to show that all $Scgn^+$ neurons are glutamatergic and express, for example, *Cck*, *Npy*, *Adcyap1*, *Cnr1*, and secretogranins (that is, neuropeptides, receptors, and SNARE components) and transcription factors (*SI Appendix*, Fig. S8*A*) in unique constellations.

We then increased understanding on how the IG integrates synaptic information by studying local connectivity: Local GABA interneurons receive significant innervation from $Scgn^+/Vglut1^+$ neurons. In contrast, $Scgn^+/Vglut1^+$ neurons themselves receive spatially segregated glutamatergic innervation along their dendrites. Interestingly, excitatory IG neurons are only sparsely interconnected, highlighting GABA interneurons as critical circuit organizers. This model of circuit organization is compatible with the finding that non-Scgn neurons (likely interneurons) are primary drug responders in the adult IG, likely precipitating significant circuit breakdown by impairment of cellular "hubs" upon psychostimulant administration. The finding that IG neurons project to the olfactory bulb is significant when considering that they express receptors for endothelin, melanin-concentrating hormone, neurotensin, and other hormones/neuropeptides, stressing that IG neurons differentially activated by a variety of brain-states could critically entrain olfactory circuits by delivering information antiparallel to olfactory output. Thus, a multimodal and reciprocal circuit emerges between olfactory and limbic areas.

Even though Scgn is a "pure" Ca^{2+} sensor given its low affinity to Ca^{2+} (73), its functional significance is only partially understood in, for example, hypothalamic neurons (47). In the IG, it is conceivable to hypothesize that Scgn postnatally can protect against runaway excitation induced by psychostimulant exposure. This notion is supported by IG neurons being drug-sensitive when lacking Scgn in utero and can have disease relevance because we consider Scgn expression to be activity-dependent as supported by 1) its distinct intracellular levels as a factor of localization (reflecting neuronal maturity) in the DG and IG and 2) limited mRNA detectability in Patch-seq–processed IG neurons ($n = 8/22$), which seems to reinforce the concept of basal expression before rapid use-dependent gene induction. Indeed, in $Scgn^{-/-}$ mice we find reduced neuronal excitability and synaptic strength, as well as significant worsening of animal behaviors coincident with the progressive development of generalized (clonic) convulsive seizures upon exposure to Meth in vivo. These data link brain-wide activity maps to a specific molecular determinant of neuronal excitability that gates the brain's vulnerability to illicit drugs. Thus, the IG is identified as a hub integrating (patho)physiological information whose therapeutic resetting might alleviate adverse psychostimulant symptomatology.

Materials and Methods

SI Appendix contains all relevant experimental procedures and protocols, specifications of reagents and materials used, and details of the statistical analysis. In this study, both fetal and adult human tissues that had been biobanked at the Medical University of Vienna and the Semmelweis University, respectively, were used. Human studies were performed with consent. Maternal consent was obtained for the use of fetal tissue. These studies conformed to the Declaration of Helsinki and approved by the Ethical Committees of the Medical University of Vienna (no.104/2009) and Semmelweis University (TUKEB 84/2014).

Data Availability Statement. All data relevant to this manuscript and available to the authors at the time of publication are included in the main text or *SI Appendix*. Specific immunoreagents or transgenic mouse models will be made available upon request to either T.G.M.H. or T.H.

ACKNOWLEDGMENTS. We thank the Biomedical Sequencing Facility at the Center for Molecular Medicine of the Austrian Academy of Sciences, particularly T. Penz and C. Bock, for assistance with next-generation sequencing and Gilberto Fisone (Karolinska Institutet) for sharing *Drd1*-GFP and *Drd2*-GFP mice. This study was supported by the National Brain Research Program of Hungary (2017-1.2.1-NKP-2017-00002, to A.A.), the Excellence Program for Higher Education of Hungary (FIKP-2018, to A.A.), the Swedish Medical Research Council (T.G.M.H. and T.H.), Swedish Brain Foundation (Hjärnfonden, T.H.), the European Research Council (ERC-2015-AdG-695136, to T.H.), and intramural funds of the Medical University of Vienna (T.H.).

1. D. Saal, Y. Dong, A. Bonci, R. C. Malenka, Drugs of abuse and stress trigger a common synaptic adaptation in dopamine neurons. *Neuron* **37**, 577–582 (2003).
2. N. D. Volkow, M. Morales, The brain on drugs: From reward to addiction. *Cell* **162**, 712–725 (2015).
3. M. Narita, M. Takagi, K. Aoki, N. Kuzumaki, T. Suzuki, Implication of Rho-associated kinase in the elevation of extracellular dopamine levels and its related behaviors induced by methamphetamine in rats. *J. Neurochem.* **86**, 273–282 (2003).
4. M. Angoa-Pérez *et al.*, Mephedrone does not damage dopamine nerve endings of the striatum, but enhances the neurotoxicity of methamphetamine, amphetamine, and MDMA. *J. Neurochem.* **125**, 102–110 (2013).
5. C. G. Silva *et al.*, Adenosine receptor antagonists including caffeine alter fetal brain development in mice. *Sci. Transl. Med.* **5**, 197ra104 (2013).
6. M. P. Kaster *et al.*, Caffeine acts through neuronal adenosine A2A receptors to prevent mood and memory dysfunction triggered by chronic stress. *Proc. Natl. Acad. Sci. U.S.A.* **112**, 7833–7838 (2015).
7. H. Takahashi *et al.*, Enhanced dopamine release by nicotine in cigarette smokers: A double-blind, randomized, placebo-controlled pilot study. *Int. J. Neuropsychopharmacol.* **11**, 413–417 (2008).
8. D. Piomelli, V. Di Marzo, Dopamine D2 receptor signaling via the arachidonic acid cascade: Modulation by cAMP-dependent protein kinase A and prostaglandin E2. *J. Lipid Mediat.* **6**, 433–443 (1993).
9. F. Abdi, I. Pollard, J. Wilkinson, Placental transfer and foetal disposition of caffeine and its immediate metabolites in the 20-day pregnant rat: Function of dose. *Xenobiotica* **23**, 449–456 (1993).
10. N. S. Shah, J. D. Yates, Placental transfer and tissue distribution of dextro-amphetamine in the mouse. *Arch. Int. Pharmacodyn. Ther.* **233**, 200–208 (1978).
11. A. M. Smith, L. P. Dwoskin, J. R. Pauly, Early exposure to nicotine during critical periods of brain development: Mechanisms and consequences. *J. Pediatr. Biochem.* **1**, 125–141 (2010).
12. X. Wang, D. Dow-Edwards, V. Anderson, H. Minkoff, Y. L. Hurd, In utero marijuana exposure associated with abnormal amygdala dopamine D2 gene expression in the human fetus. *Biol. Psychiatry* **56**, 909–915 (2004).
13. B. J. Cord *et al.*, Characterization of axon guidance cue sensitivity of human embryonic stem cell-derived dopaminergic neurons. *Mol. Cell. Neurosci.* **45**, 324–334 (2010).
14. D. Hoops, C. Flores, Making dopamine connections in adolescence. *Trends Neurosci.* **40**, 709–719 (2017).
15. C. J. Guenthner, K. Miyamichi, H. H. Yang, H. C. Heller, L. Luo, Permanent genetic access to transiently active neurons via TRAP: Targeted recombination in active populations. *Neuron* **78**, 773–784 (2013).
16. P. Rakic, Adult neurogenesis in mammals: An identity crisis. *J. Neurosci.* **22**, 614–618 (2002).
17. A. Duque, Z. Krsnik, I. Kostović, P. Rakic, Secondary expansion of the transient subplate zone in the developing cerebrum of human and nonhuman primates. *Proc. Natl. Acad. Sci. U.S.A.* **113**, 9892–9897 (2016).
18. D. Calvigioni *et al.*, Functional differentiation of cholecystokinin-containing interneurons destined for the cerebral cortex. *Cereb. Cortex* **27**, 2453–2468 (2017).
19. T. Hökfelt, A. Ljungdahl, K. Fuxe, O. Johansson, Dopamine nerve terminals in the rat limbic cortex: Aspects of the dopamine hypothesis of schizophrenia. *Science* **184**, 177–179 (1974).
20. J. Mulder *et al.*, Secretagogin is a Ca2+-binding protein specifying subpopulations of telencephalic neurons. *Proc. Natl. Acad. Sci. U.S.A.* **106**, 22492–22497 (2009).
21. R. S. Tubbs, M. Prekupec, M. Loukas, E. M. Hattab, A. A. Cohen-Gadol, The indusium griseum: Anatomic study with potential application to callosotomy. *Neurosurgery* **73**, 312–315, discussion 316 (2013).
22. I. Matějovská, K. Bernášková, R. Šlamberová, Effect of prenatal methamphetamine exposure and challenge dose of the same drug in adulthood on epileptiform activity induced by electrical stimulation in female rats. *Neuroscience* **257**, 130–138 (2014).
23. K. Bernaskova, S. Tomkova, R. Slamberova, Are changes in excitability in the hippocampus of adult male rats induced by prenatal methamphetamine exposure or stress? *Epilepsy Res.* **137**, 132–138 (2017).
24. N. Aronin, S. M. Sagar, F. R. Sharp, W. J. Schwartz, Light regulates expression of a Fos-related protein in rat suprachiasmatic nuclei. *Proc. Natl. Acad. Sci. U.S.A.* **87**, 5959–5962 (1990).

Downloaded at Palestinian Territory, occupied on November 30, 2021
www.manaraa.com

25. H. J. Bennett, K. Semba, Immunohistochemical localization of caffeine-induced c-Fos protein expression in the rat brain. *J. Comp. Neurol.* **401**, 89–108 (1998).
26. A. Groves *et al*., A functionally defined *in vivo* astrocyte population identified by c-Fos activation in a mouse model of multiple sclerosis modulated by S1P signaling: Immediate-early astrocytes (*ieAstrocytes*). *eNeuro* **5**, ENEURO.0239-18.2018 (2018).
27. L. R. Reznikov, R. K. Pasumarthi, J. R. Fadel, Caffeine elicits c-Fos expression in horizontal diagonal band cholinergic neurons. *Neuroreport* **20**, 1609–1612 (2009).
28. A. Carmena *et al*., Methamphetamine-induced toxicity in indusium griseum of mice is associated with astro- and microgliosis. *Neurotox. Res.* **27**, 209–216 (2015).
29. S. Jayanthi, X. Deng, P. A. Noailles, B. Ladenheim, J. L. Cadet, Methamphetamine induces neuronal apoptosis via cross-talks between endoplasmic reticulum and mitochondria-dependent death cascades. *FASEB J.* **18**, 238–251 (2004).
30. J. F. Wilson *et al*., Effects of low doses of caffeine on aggressive behavior of male rats. *Psychol. Rep.* **86**, 941–946 (2000).
31. E. C. Jobli, S. E. Gardner, A. B. Hodgson, A. Essex, The review of new evidence 5 years later: SAMHSA's national registry of evidence-based programs and practices (NREPP). *Eval. Program Plann.* **48**, 117–123 (2015).
32. M. C. Brucker, T. L. King, The 2015 US food and drug administration pregnancy and lactation labeling rule. *J. Midwifery Womens Health* **62**, 308–316 (2017).
33. Y. Edling, M. Ingelman-Sundberg, A. Simi, Glutamate activates c-fos in glial cells via a novel mechanism involving the glutamate receptor subtype mGlu5 and the transcriptional repressor DREAM. *Glia* **55**, 328–340 (2007).
34. A. Alvarez-Buylla, J. M. García-Verdugo, A. D. Tramontin, A unified hypothesis on the lineage of neural stem cells. *Nat. Rev. Neurosci.* **2**, 287–293 (2001).
35. B. Rusak, L. McNaughton, H. A. Robertson, S. P. Hunt, Circadian variation in photic regulation of immediate-early gene mRNAs in rat suprachiasmatic nucleus cells. *Brain Res. Mol. Brain Res.* **14**, 124–130 (1992).
36. Z. Henderson *et al*., Somato-dendritic nicotinic receptor responses recorded in vitro from the medial septal diagonal band complex of the rodent. *J. Physiol.* **562**, 165–182 (2005).
37. N. Francis *et al*., NT-3, like NGF, is required for survival of sympathetic neurons, but not their precursors. *Dev. Biol.* **210**, 411–427 (1999).
38. F. Laplante, O. Mnie-Filali, R. M. Sullivan, A neuroanatomical and neurochemical study of the indusium griseum and anterior hippocampal continuation: Comparison with dentate gyrus. *J. Chem. Neuroanat.* **50-51**, 39–47 (2013).
39. K. T. Muneoka, M. Takigawa, 5-Hydroxytryptamine7 (5-HT7) receptor immunoreactivity-positive 'stigmoid body'-like structure in developing rat brains. *Int. J. Dev. Neurosci.* **21**, 133–143 (2003).
40. Y. Sugitani *et al*., Brn-1 and Brn-2 share crucial roles in the production and positioning of mouse neocortical neurons. *Genes Dev.* **16**, 1760–1765 (2002).
41. A. Mouatt-Prigent, Y. Agid, E. C. Hirsch, Does the calcium binding protein calretinin protect dopaminergic neurons against degeneration in Parkinson's disease? *Brain Res.* **668**, 62–70 (1994).
42. D. Ferrari *et al*., Neuroprotective activity of omega-3 fatty acids against epilepsy-induced hippocampal damage: Quantification with immunohistochemical for calcium-binding proteins. *Epilepsy Behav.* **13**, 36–42 (2008).
43. B. Schwaller, M. Meyer, S. Schiffmann, 'New' functions for 'old' proteins: The role of the calcium-binding proteins calbindin D-28k, calretinin and parvalbumin, in cerebellar physiology. Studies with knockout mice. *Cerebellum* **1**, 241–258 (2002).
44. E. Neher, T. Sakaba, Multiple roles of calcium ions in the regulation of neurotransmitter release. *Neuron* **59**, 861–872 (2008).
45. J. Attems *et al*., Clusters of secretagogin-expressing neurons in the aged human olfactory tract lack terminal differentiation. *Proc. Natl. Acad. Sci. U.S.A.* **109**, 6259–6264 (2012).
46. J. Attems *et al*., Immunoreactivity of calcium binding protein secretagogin in the human hippocampus is restricted to pyramidal neurons. *Exp. Gerontol.* **42**, 215–222 (2007).
47. R. A. Romanov *et al*., Molecular interrogation of hypothalamic organization reveals distinct dopamine neuronal subtypes. *Nat. Neurosci.* **20**, 176–188 (2017).
48. J. Fuzik *et al*., Integration of electrophysiological recordings with single-cell RNA-seq data identifies neuronal subtypes. *Nat. Biotechnol.* **34**, 175–183 (2016).
49. J. Attems *et al*., Calcium-binding protein secretagogin-expressing neurones in the human hippocampus are largely resistant to neurodegeneration in Alzheimer's disease. *Neuropathol. Appl. Neurobiol.* **34**, 23–32 (2008).
50. L. H. Lin *et al*., Localization of vesicular glutamate transporters and neuronal nitric oxide synthase in rat nucleus tractus solitarii. *Neuroscience* **123**, 247–255 (2004).
51. R. Martín-Ibañez *et al*., Vesicular glutamate transporter 3 (VGLUT3) identifies spatially segregated excitatory terminals in the rat substantia nigra. *Eur. J. Neurosci.* **23**, 1063–1070 (2006).
52. E. A. Susaki *et al*., Whole-brain imaging with single-cell resolution using chemical cocktails and computational analysis. *Cell* **157**, 726–739 (2014).
53. G. D. Adamek, M. T. Shipley, M. S. Sanders, The indusium griseum in the mouse: Architecture, Timm's histochemistry and some afferent connections. *Brain Res. Bull.* **12**, 657–668 (1984).
54. K. Malenczyk *et al*., A TRPV1-to-secretagogin regulatory axis controls pancreatic β-cell survival by modulating protein turnover. *EMBO J.* **36**, 2107–2125 (2017).
55. T. Matsuzaki *et al*., The responses of hypothalamic NPY and OBRb mRNA expression to food deprivation develop during the neonatal-prepubertal period and exhibit gender differences in rats. *Int. J. Dev. Neurosci.* **41**, 63–67 (2015).
56. B. Tasic *et al*., Adult mouse cortical cell taxonomy revealed by single cell transcriptomics. *Nat. Neurosci.* **19**, 335–346 (2016).
57. T. Iwano, A. Masuda, H. Kiyonari, H. Enomoto, F. Matsuzaki, Prox1 postmitotically defines dentate gyrus cells by specifying granule cell identity over CA3 pyramidal cell fate in the hippocampus. *Development* **139**, 3051–3062 (2012).
58. S. Y. Branch, M. J. Beckstead, Methamphetamine produces bidirectional, concentration-dependent effects on dopamine neuron excitability and dopamine-mediated synaptic currents. *J. Neurophysiol.* **108**, 802–809 (2012).
59. S. Jayanthi *et al*., Methamphetamine downregulates striatal glutamate receptors via diverse epigenetic mechanisms. *Biol. Psychiatry* **76**, 47–56 (2014).
60. J. P. Zhu, W. Xu, J. A. Angulo, Methamphetamine-induced cell death: Selective vulnerability in neuronal subpopulations of the striatum in mice. *Neuroscience* **140**, 607–622 (2006).
61. T. C. Lin, L. T. Huang, Y. N. Huang, G. S. Chen, J. Y. Wang, Neonatal status epilepticus alters prefrontal-striatal circuitry and enhances methamphetamine-induced behavioral sensitization in adolescence. *Epilepsy Behav.* **14**, 316–323 (2009).
62. F. J. Kane, Jr, M. H. Keeler, C. B. Reifler, Neurological crises following methamphetamine. *J. Am. Med. Assoc.* **210**, 556–557 (1969).
63. T. Wang, J. Wang, J. E. Cottrell, I. S. Kass, Small physiologic changes in calcium and magnesium alter excitability and burst firing of CA1 pyramidal cells in rat hippocampal slices. *J. Neurosurg. Anesthesiol.* **16**, 201–209 (2004).
64. J. H. Xu, F. R. Tang, Voltage-dependent calcium channels, calcium binding proteins, and their interaction in the pathological process of epilepsy. *Int. J. Mol. Sci.* **19**, E2735 (2018).
65. D. C. Rogers *et al*., Behavioral and functional analysis of mouse phenotype: SHIRPA, a proposed protocol for comprehensive phenotype assessment. *Mamm. Genome* **8**, 711–713 (1997).
66. D. C. Rogers *et al*., SHIRPA, a protocol for behavioral assessment: Validation for longitudinal study of neurological dysfunction in mice. *Neurosci. Lett.* **306**, 89–92 (2001).
67. A. Alpár, T. Harkany, Novel insights into the spatial and temporal complexity of hypothalamic organization through precision methods allowing nanoscale resolution. *J. Intern. Med.* **284**, 568–580 (2018).
68. G. La Manno *et al*., Molecular diversity of midbrain development in mouse, human, and stem cells. *Cell* **167**, 566–580.e19 (2016).
69. A. Zeisel *et al*., Molecular architecture of the mouse nervous system. *Cell* **174**, 999–1014.e22 (2018).
70. R. R. Sturrock, Development of the indusium griseum. II. A semithin light microscopic and electron microscopic study. *J. Anat.* **125**, 433–445 (1978).
71. R. R. Sturrock, Development of the indusium griseum. III. An autoradiographic study of cell production. *J. Anat.* **126**, 1–6 (1978).
72. A. Faissner, N. Heck, A. Dobbertin, J. Garwood, DSD-1-Proteoglycan/Phosphacan and receptor protein tyrosine phosphatase-beta isoforms during development and regeneration of neural tissues. *Adv. Exp. Med. Biol.* **557**, 25–53 (2006).
73. A. Rogstam *et al*., Binding of calcium ions and SNAP-25 to the hexa EF-hand protein secretagogin. *Biochem. J.* **401**, 353–363 (2007).

Downloaded at Palestinian Territory, occupied on November 30, 2021

www.manaraa.com